Supplementary Information

Mechanochemical transformation of spent ternary lithium-ion battery electrode material to perovskite oxides for catalytic CO oxidation

Guangze Nie [a, §], *Xiangqian Du* [b, §], *Hongchao Yu* [b], *Weiyi Fan* [b], *Min Pan* [b], *Fei Gao* [b], *Feng Wu* [b], *Yunchuan Hong* [b], *Hongjian Tang* [a], *Zhihao Zhou* [a], *Guoshu Deng* [a], *Lin Li* [a], *Zhenkun Sun* [a, *], *and Lunbo Duan* [a, *]

[a] Key Laboratory of Energy Thermal Conversion and Control, Ministry of Education, School of Energy and Environment, Southeast University, Nanjing, 210096, China.

[b] MCC Huatian Engineering and Technology Corporation, Nanjing, 210019, China

[§] These authors contributed equally to this study.

* Corresponding authors: zhenkun_sun@seu.edu.cn, duanlunbo@seu.edu.cn

Contents

1 EXPERIMENT SECTION

1.1 Catalyst preparation

1.1.1 Preparation of LNCM-SG-R

The LNCM-SG-R catalyst was prepared by recycling NCM elements from LIBs via a conventional wet synthesis (sol-gel method). In particular, 1.2 g NCMO powder was first completely dissolved in 25 ml dilute nitric acid (2.5 mol /L) at 50 °C in a water bath. And then, 1.5 times of the stoichiometric molar amount of citric acid and same molar amount of $La(NO_3)_3 \cdot 6H_2O$ (AR) as that of metals contained the dissolved solution were added into the nitric acid solution in the last step. After that, the mixture was stirred vigorously at 90 ℃ in water bath until most of the water was evaporated and then the mixture was dried at 120 ℃ oven overnight. At final, the mixture was calcined as follows: firstly, it was heated up to 260 °C at a rate of 2 °C·min^{-1} and kept at 200 °C for 120 min; secondly, it was heated up to 750 °C at a rate of 2 °C·min^{-1} and held at 750 °C for 300 min in air atmosphere.

1.1.2 Preparation of LNCM-SG-C

The LNCM-SG-C catalyst was prepared from commercial chemicals by a conventional sol-gel method. Typically, 0.015 mol $Ni(NO_3)_2 \cdot 6H_2O$, 0.005 mol $Co(NO_3)_2 \cdot 6H_2O$ and 0.005 mol $Mn(NO_3)_2 \cdot 4H_2O$ and 0.025 mol $La(NO_3)_3 \cdot 6H_2O$ were dissolved into 25 ml deionized water. Then, 0.0375 mol citric acid were added in the

solution. After that, the mixture was stirred vigorously at 90 ℃ in water bath until most of the water was evaporated and then the mixture was dried at 120 ℃ oven overnight. At final, the mixture was calcined as follows: firstly, it was heated up to 260 °C at a rate of 2 °C·min^{-1} and kept at 200 °C for 120 min; secondly, it was heated up to 750 °C at a rate of 2 °C·min^{-1} and held at 750 °C for 300 min in air atmosphere.

1.2 Material characterization

Inductively coupled plasma optical emission spectrometry (ICP-OES, Thermo Fisher Scientific ICAP PRO) was used to investigate the contents of Ni, Co, Mn, Li and Al elements in the NCM.

The phase and unit cell structures of the synthesized catalyst were analyzed by powder X-ray diffraction (XRD) technique. XRD analysis was carried out on an Rigaku Ultimate IV powder X-ray radiation diffractometer, Japan, equipped with Cu Kα radiation = 1.5418 Å, with a scan rate of 2° min^{-1}. The obtained XRD pattern was compared with a standard card to obtain the phase composition of the catalyst. Crystallite size of the products is calculated from the full width at half maximum of the XRD diffraction peaks at $2\theta \approx 47°$ for perovskites and 43° for NiO by using the Scherrer's equation:

$$D = \frac{k \cdot \lambda}{B \cdot \cos\theta} \quad \text{(S1)}$$

where D is the crystallite size, λ is the X-ray wavelength of 1.54 Å, B is the full width at half maximum of the diffraction line, h is the angle of diffraction, k is a constant (having the value 0.9 in our case).

The morphology and microstructure of the catalyst were directly observed by field emission environment scanning electron microscopy (SEM) produced by Hitachi, Japan (Regulus 8100) and transmission electron microscope (TEM) produced by Thermo Fisher Scientific, USA (Talos F200X).

The specific surface area of the catalyst was analyzed by N_2 adsorption-desorption, which was carried out on Micromeritics APSP 2460.

X-ray photoelectron spectroscopy (XPS) is mainly used to analyze the surface element composition, valence charge and species of the catalyst. The K-Alpha type XPS produced by Thermo Fisher Scientific of the USA uses Al Kα (h_v = 1486.6 eV) as the excitation source and C 1s (284.8 eV) as the standard to calibrate the other elements.

The thermal analysis of the catalysts after 20-hour long-term stability test were studied using thermogravimetric-infrared (TG-IR) analysis. The experimental setup employed a simultaneous thermal analyzer (TA Instruments SDT 650) and Fourier-transform infrared (FTIR, Nicolet IS 20) spectrometer. The system combines thermal analysis with infrared spectroscopy of CO_2. Thermal analysis of the used catalysts was conducted in an air flow of 100 ml min^{-1} within a heating rate of 10 °C min^{-1} in the temperature range of 100 - 850 °C. The preliminary measurement of the empty crucible was utilized as the background data. The absorption band at 2361 cm^{-1} in FTIR spectra was employed for the analysis of CO_2, throughout the temperature range of the thermal analysis.

Electron spin resonance (ESR) spectra were acquired on a Bruker ESR 5000 spectrometer (USA) operating in the X-band. To detect the presence and amount of oxygen vacancies on catalysts, the ESR measurement was carried out in high vacuum after the samples were pretreated in N_2 at 400 °C to remove surface adsorbed oxygen species.

The temperature-programmed desorption of O_2 temperature-programmed desorption (O_2-TPD) and H_2 temperature-programmed reduction (H_2-TPR) experiments over all samples were conducted in a AutoChem II 2920 (Micromeritics, USA). Before each of the experiments, the samples (100 mg) were pretreated in flowing He (50 mL/min) at 200 °C for 1 h, followed by cooling down to room temperature. For O_2-TPD, the pretreated sample (100 mg) was exposed to 4% O_2/He (50 mL/min) at room temperature for 30 min and then ramped (10 °C/min) up to 800 °C in He. For H_2-TPR, the reduction of pretreated samples (100 mg) was carried out from room temperature to 800 °C in a flow of 10% H_2/He (50 mL min^{-1}) at the ramping of 10 °C min^{-1}. The gas stream was monitored by a thermal conductivity detector (TCD).

The in situ diffuse reflectance infrared transform spectroscopy (DIRFTS) of CO oxidation was carried out using a Bruker INVENIO-S (German)spectrometer equipped with an MCT detector. Prior to the DIRFTS measurement, the samples were purged with N_2 at 370 °C (on the basis of O_2-TPD results) for 30 min to remove surface-adsorbed oxygen species as much as possible. Then cooling to 200 °C for 30 min, the backgrounds were collected at 200 °C in a N_2 flow. Afterward, a flow of 1% CO/N_2, 5% O_2/N_2, and 1% CO+5% O_2/N_2 was successively fed onto the pretreated catalyst surface and held for 30 min at 200 °C, respectively. The spectra were collected simultaneously. All total gas flow is 50 mL/min.

1.3 Catalytic performance evaluation

The temperature-programmed oxidation of CO was employed to evaluate the activity of catalytic CO removal. A 0.4 g catalyst (0.3 – 0.45 mm) was put in a fixed-bed reactor with a 10 mm inner diameter quartz tube. The reactant gas was 1 vol% CO and 15 vol% O_2 carried by N_2. The total flow gas was 200 ml min^{-1} (30,000 ml $g^{-1}h^{-1}$). After the gas concentration was stable, the temperature was increased with the rate of 10 °C·min^{-1}. The outlet gas was analyzed employing an infrared flue gas analyzer (MRU VARIO PLUS). CO conversion (X_{CO}, %) was defined as $(C_i\text{-}C_o)/C_i\times100\%$, where C_i and C_o are CO concentration corresponding to the inlet and outlet, respectively. The catalytic activity was evaluated by the values of T_{50} and T_{90}, which were defined as the temperatures at 50% and 90% of CO conversion, respectively. In addition, the reaction rate (r_{norm}, mol $s^{-1}m^{-2}$) is derived from the following Eq. S2:

$$r_{norm} = \frac{C_i \cdot F \cdot X_{CO}}{m \cdot S_{BET}} \quad \text{(S2)}$$

Where F (mol h^{-1}) is the gas flow rate, the m is the mass of catalyst, S_{BET} is measured by N_2 adsorption-desorption analysis.

The apparent activation energie of oxidation reaction (E_a, kJ mol^{-1}) is calculated based on the Arrhenius equation, on the condition of X_{CO} lower than 10% to reduce the effect of mass transfer:

$$\mathrm{Ln}(r)=\frac{E_a}{RT}-\mathrm{Ln}(A) \qquad \text{(S3)}$$

1.4 Economic and environmental analysis

The EverBatt model[1], developed by the Argonne National Laboratory, was employed to conduct a techno-economic and life-cycle assessment of recycling spent batteries. This comprehensive model is designed to evaluate the costs and environmental implications of battery recycling processes. In addition, our assessment has added necessary perovskite synthesis processes after recycling spent LIBs. The analysis focused on the total energy use, greenhouse gas (GHG) emissions, and economic value of the three synthesis methods[2].

The synthesis process of LNCMO-16-600, which represents the process of solid-state recovery of lithium batteries to prepare perovskite, is shown in Figure S17a. spent LIBs are shredded, and then undergo a low temperature calcination process to burn off the binder and electrolyte, several physical separation processes to separate out aluminum, copper, steel as metal scraps and plastics, and a leaching process followed by hydrogen reduction, extraction and precipitation to produce lithium hydroxide, and Ni/Co/Mn compounds for perovskite production. The calcined Ni/Co/Mn compounds is milled and calcined after mixing with La source to form perovskite

During the traditional wet synthesis of LNCM-SG-R by recycling lithium batteries through hydrometallurgical methods (Figure S17b), the first step is the disassembly process. The cathode powders are separated after disassembling. Then, the metal oxides are leached into metal ions by using chemical reagents such as acid and alkali. Ni/Co/Mn metal salts,

obtained through alkaline precipitation, is used as precursor to synthesize perovskite via sol-gel method.

The typical sol-gel method is also used in the synthesis of LNCM-SG-C (Figure S17c), and the difference from LNCM-SG-R is that all raw materials are commercial chemicals.

1.4.1 Evaluation of the life-cycle total energy consumption and GHG emissions

The three synthesis processes of perovskite oxides, featuring LNCMO-16-600, LNCM-SG-R, LNCM-SG-C respectively, are assumed to be based on processing 1,000 metric tons of perovskite catalysts per year in China. The modeling of the life-cycle total energy and GHG emissions was based on the materials and energy flows through the LIBs recycling and perovskite fabrication process, as discussed below.

Materials input: The materials requirements for the three recycling technologies are summarized in Table S8. The materials requirements for the spent LIBs recycling processes are obtained from EverBatt, and the materials requirements for the perovskite synthesis process are obtained based on our lab process. The life-cycle analysis accounts for the environmental impacts of all the materials consumed in the process by capturing the environmental impacts associated with their upstream production.

Energy input: To calculate the life-cycle environmental impacts attributable to all types of energy consumed in the process, the life-cycle analysis considers the environmental impacts associated with electricity generation, as well as those associated

with on-site fuel combustion (Table S9). The purchased energy consumptions for the spent LIBs recycling processes are obtained from EverBatt, while that for the perovskite synthesis process is estimated from calculations based on our lab process.

Process emissions: In the life-cycle analysis, we also accounted for environmental impacts associated with process emissions that are not due to fuel combustion. For the three synthesis processes, process emissions include those from material combustion and thermal decomposition.

1.4.2 Cost and co-products revenue analysis

The specific cost parameters chosen for the industry manufacturing plant are summarized in Table S10. The co-products revenue calculation was based on the sales of recycled materials in LIBs recycling process. The prices are listed in Table S11.

2 SUPPORTING FIGURES AND TABLES

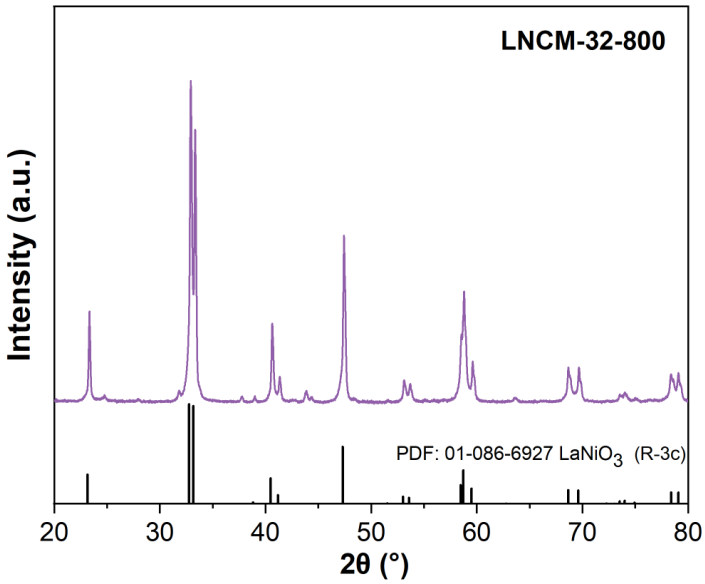

Fig.S1 XRD pattern of LNCM-32-800

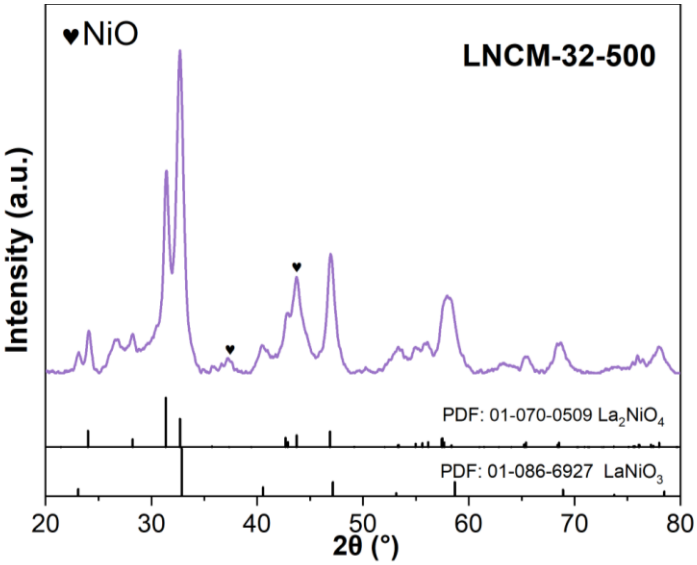

Fig.S2 XRD pattern of LNCM-32-800

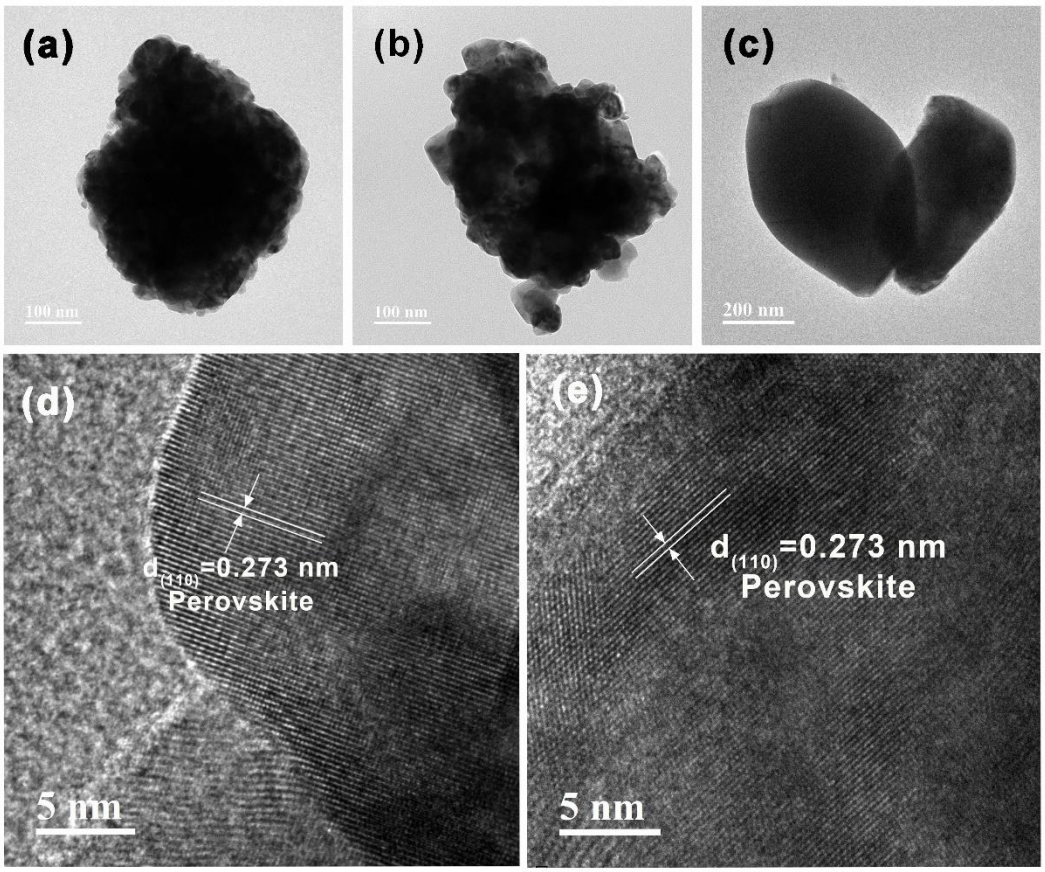

Fig.S3 TEM images of (a) LNCM-16-600, (b) LNCM-16-800, (c) LNCM-16-1000, and HRTEM images of (d) LNCM-16-800, and (e) LNCM-16-1000.

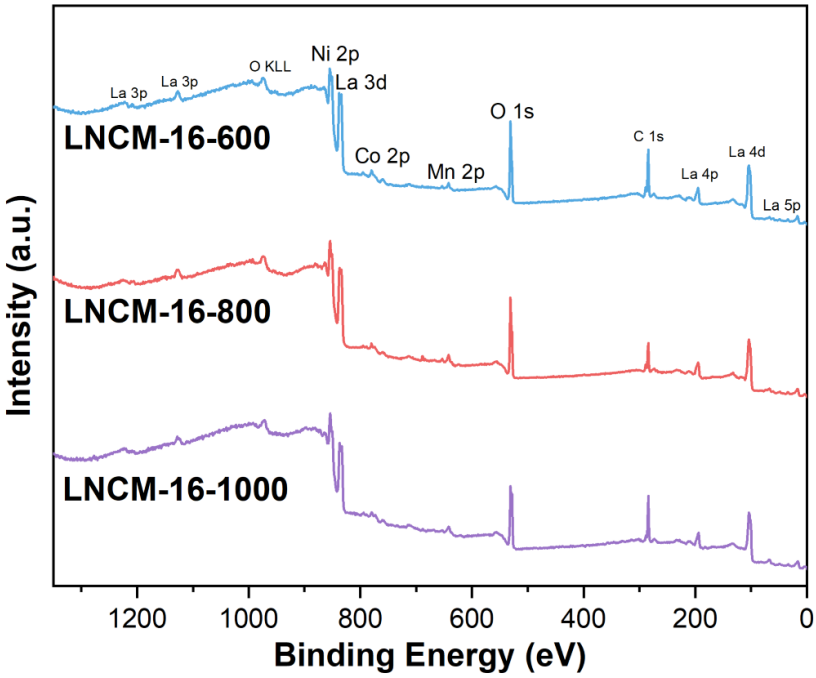

Fig.S4 XPS survey over catalysts LNCM-16-600, LNCM-16-800 and LNCM-16-1000.

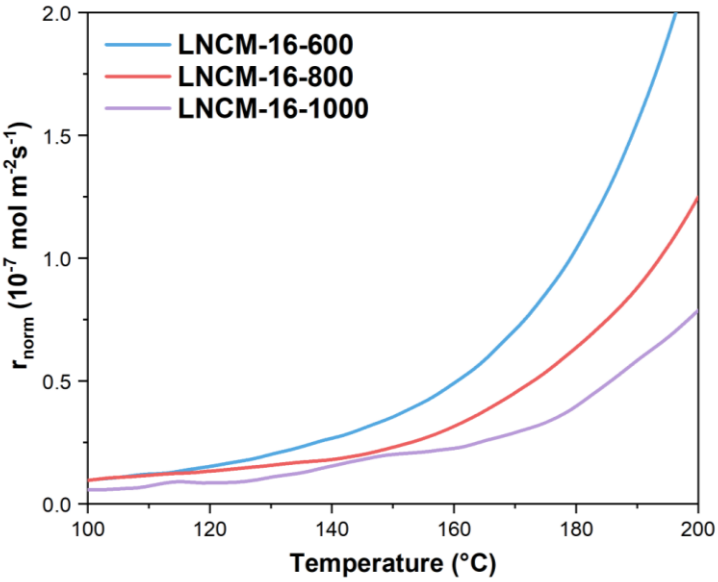

Fig.S5 Normalized CO conversion rate (r_{norm}) versus temperature over catalysts LNCM-16-600, LNCM-16-800 and LNCM-16-1000

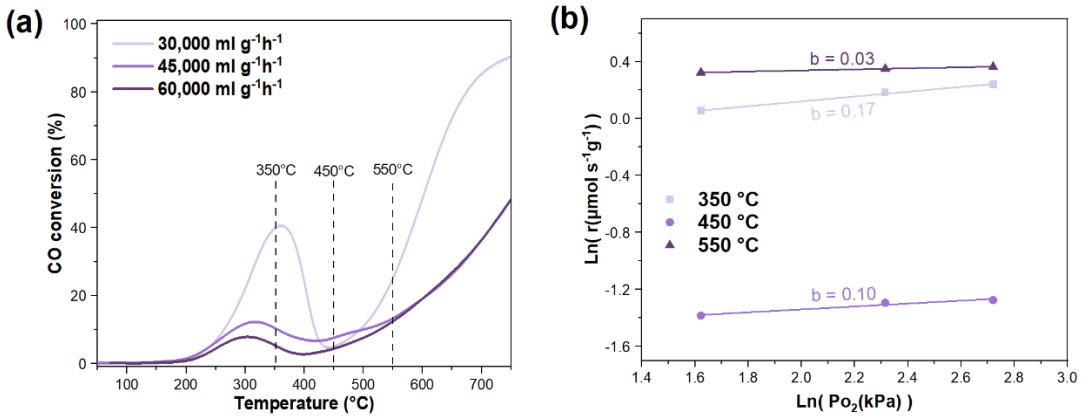

Fig.S6 (a) Light-off curves during CO oxidation over catalyst LNCM-16-1000 under different WHSVs; (b) dependence of CO reaction rate on partial pressure of O_2 over catalyst LNCM-16-1000 catalyst (WHSV = 45,000 ml $g^{-1}h^{-1}$).

Fig.S6 (a) shows the light-off curves of the CO oxidation over LNCM-16-1000 under different WHSVs. The reaction condition is 1% CO, 15% O_2 and 84% N_2. Although the CO conversion decreases with increases in WHSV from 30,000 to 60,000 ml $g^{-1}h^{-1}$, the CO conversion continues to decline with elevated temperatures (300 to 450 °C), indicating that mass transfer limitation is not the primary factor.

Another explanation is that the active sites involved in the catalytic reaction differ at different temperatures, leading to changes in catalytic performance. To verify the hypothesis, Fig. S6(b) shows how the rates of CO oxidation changed under different temperature (350,450 and 550 °C) as a function of the partial pressure of O_2 demonstrating that different oxygen species play a significantly varied role in the catalytic reaction. The

order of the b values at the three temperatures is 350 °C (0.17) > 450 °C (0.10) > 550 °C (0.03), indicating that the CO oxidation mechanism over LNCM-16-1000 catalyst may gradually changes from the mixed mechanism of L-H and MvK at 350 °C to a typical MvK mechanism at 550 °C (for a more detailed explanation, please refer to the caption of Figure S13.). For LNCM-16-1000 catalyst, the L-H mechanism is impressed and MvK mechanism is not fully activated at 450 °C, which results in a decrease in CO conversion. A change in reaction mechanism is frequently attributed to a variation in the active sites.[3] Therefore, the active sites involved in the catalytic reaction differ at varying temperatures, is the most possible reason for the changes in catalytic performance.

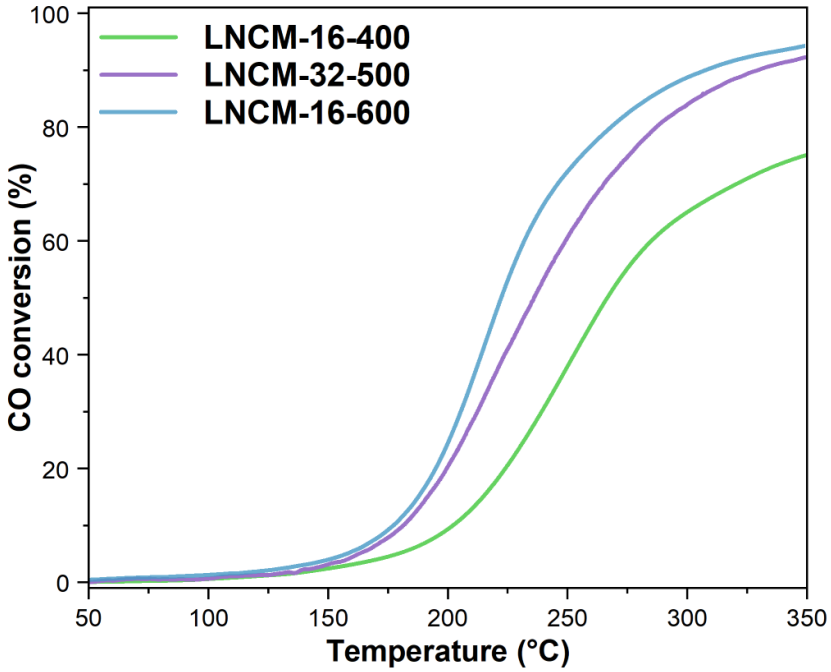

Fig.S7 Light-off curves during CO oxidation over catalysts LNCM-16-400, LNCM-32-500 and LNCM-16-600.

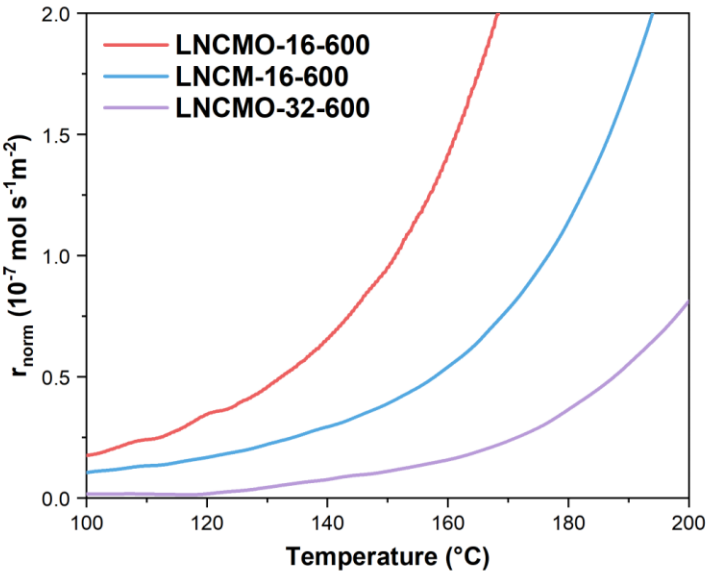

Fig.S8 Normalized CO conversion rate (r_{norm}) versus temperature over catalysts LNCMO-16-600, LNCM-16-600 and LNCMO-32-600.

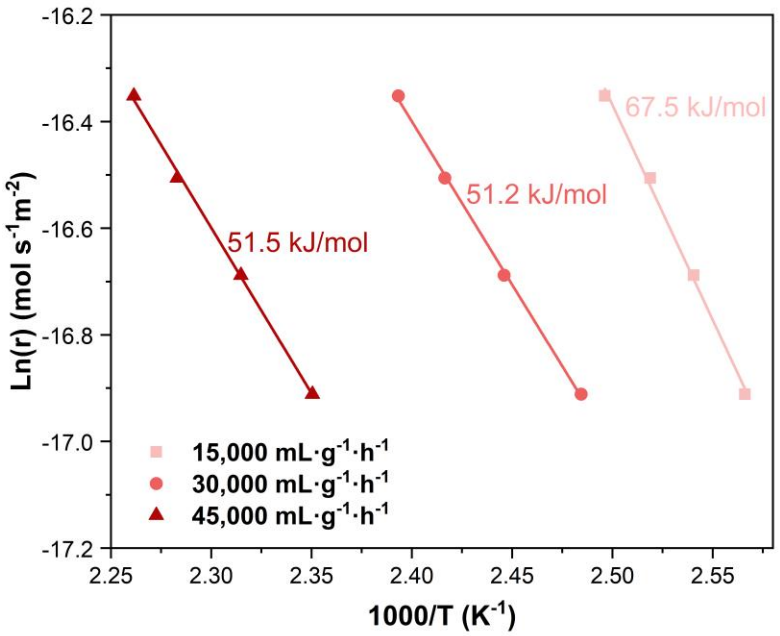

Fig.S9 Arrhenius plots for catalytic CO oxidation over catalyst LNCMO-16-600 under different WHSVs.

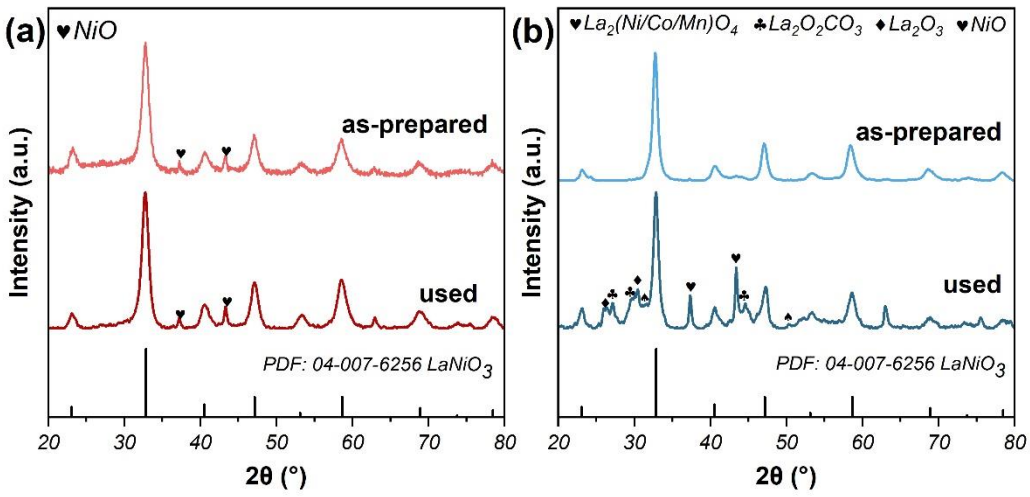

Fig.S10 XRD patterns for the as-prepared and used catalysts of (a) LNCMO-16-600 and (b) LNCM-16-600

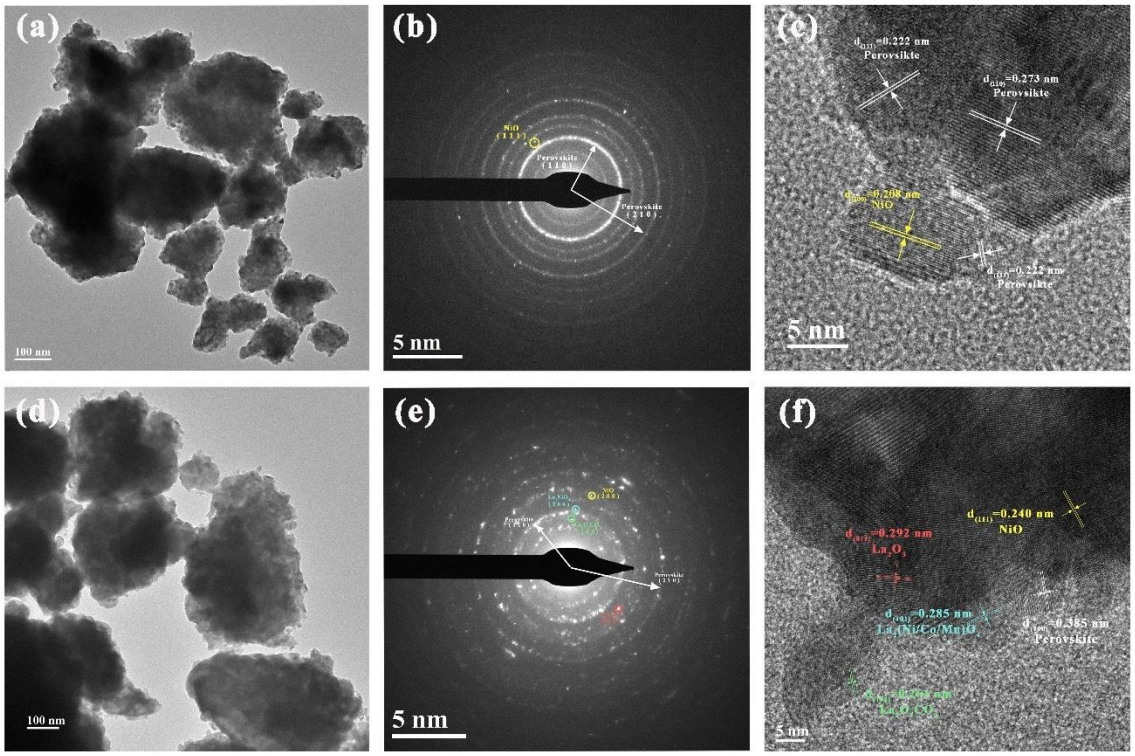

Fig.S11 (a) TEM image at low magnification, (b) SAED image and and (c) HRTEM image taken on used LNCMO-16-600 catalyst; (d) TEM image at low magnification, (e)SAED image and (f) HRTEM image taken on used LNCMO-16-600 catalyst.

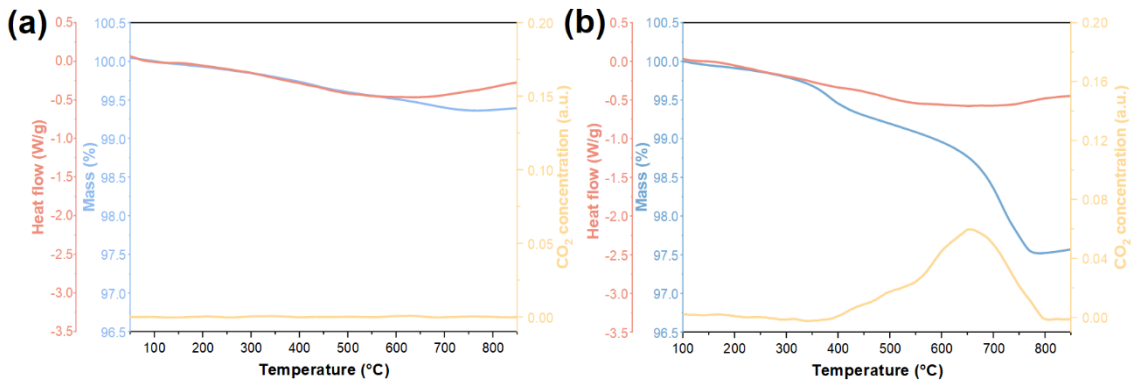

Fig.S12 TG-IR obtained at a heating rate of 10 °C/min in an air flow of 100 mL/min of used (a) LNCMO-16-600 and (b) LNCM-16-600 samples

The TG-IR analysis results of the used LNCMO-16-600 and the used LNCM-16-600 are presented in Fig.S12(a) and (b), respectively. For used LNCMO-16-600, when temperature raise from 100 °C to 750 °C， the mass only slightly decreased from 100% to 99.3%. The negative value of heat flow in the temperature range of 100-850 °C indicate a heat-absorbing process. At temperatures exceeding 600 °C, the heat flow increases gradually with temperature. It may be due to a transformation in the perovskite structure which undergoes a shift from cubic (in the Pm-3m space group) to rhombohedral (in the R-3c space group), as previously discussed (Fig.2 (C)). The absence of significant CO_2 detection throughout heating process, indicates that neither carbon deposition nor carbonate accumulation occurred. In conjunction with the XRD (Fig.10(a)) and TEM (Fig.11(a)) results, it can be posited that LNCMO-16-600 catalyst remains unaltered during 20-hour test, exhibiting remarkable stability. For the LNCM-16-600 catalyst, a significant

decline in mass was observed following an increase in temperature to 400 °C, with a reduction to 97.6% at 760 °C. Furthermore, the production of CO_2 gas is also detected at temperatures exceeding 400 °C. The heat flow curve shows no exothermic peak, indicating that production of CO_2 is not due to the oxidation of carbon deposits. As evidenced by the XRD (Fig.10(b)) and TEM(Fig.11(b)) analysis, as well as in accordance with and literature,[4] the released CO_2 is derived from the decomposition of $La_2O_2CO_3$. The LNCM-16-600 catalyst underwent perovskite structure decomposition and carbonate accumulation during the 20-hour stability test.

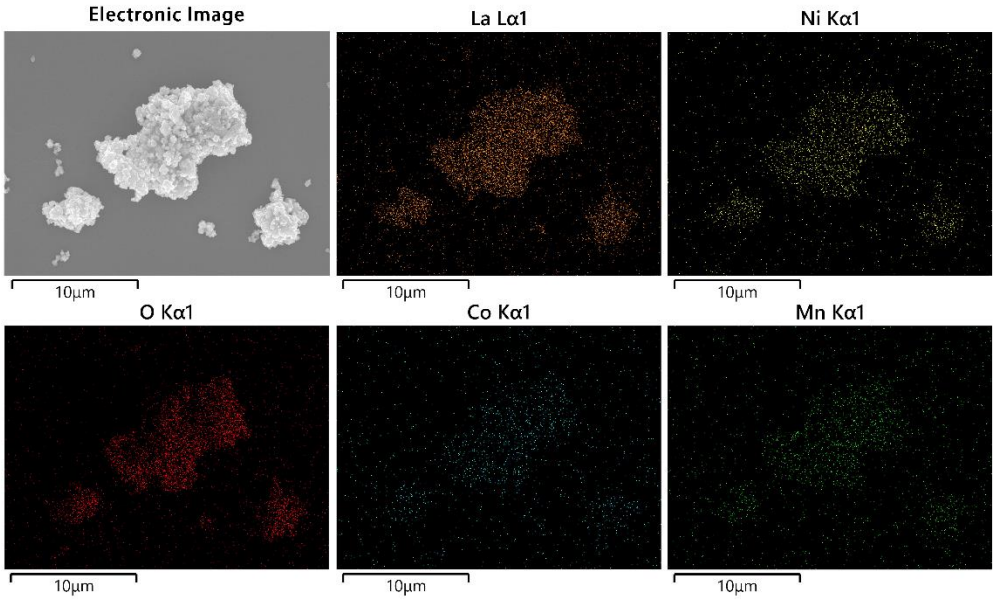

Fig.S13 SEM-EDS elemental mapping images taken on catalyst LNCMO-16-600.

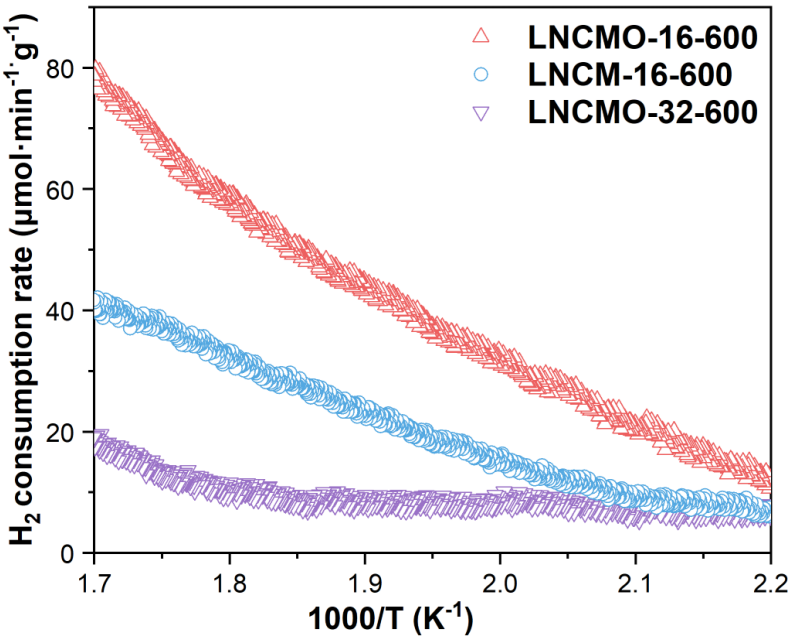

Fig.S14 The initial H_2 consumption rate as a function of inverse temperature over different catalysts.

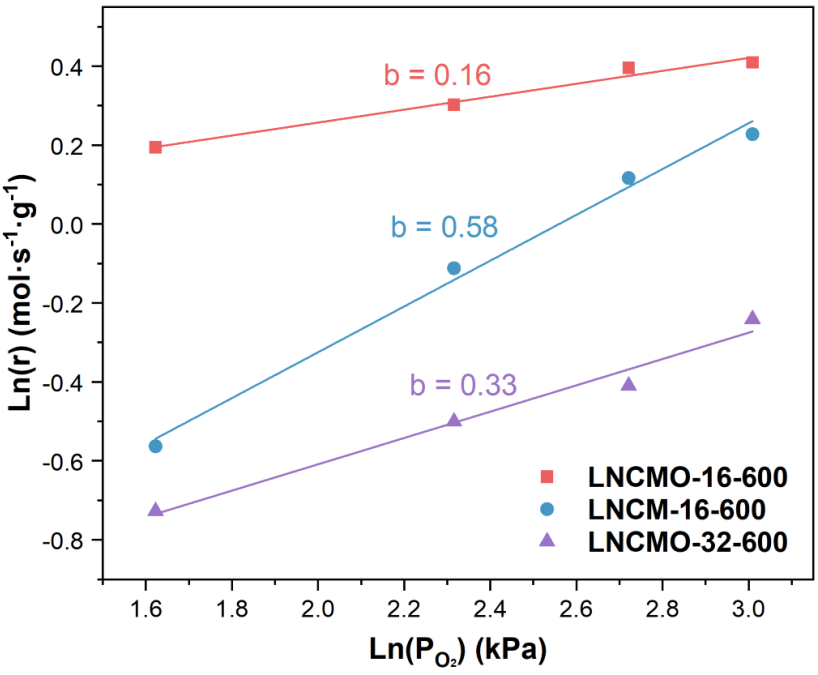

Fig.S15 Dependence of reaction rate on partial pressure of O_2 over catalysts LNCMO-16-600, LNCM-16-600 and LNCMO-32-600.

The reaction rate be expressed as the equations below:

$$r = k\, P_{CO}^{a}\, P_{O_2}^{b} \tag{S4}$$

$$Ln(r) = Ln(k) + a\, Ln(P_{co}) + b\, Ln\left(P_{O_2}\right) \tag{S5}$$

Where r is the reaction rate (μmol $g^{-1}s^{-1}$); k is the rate constant associated with E_a; P_{CO} and P_{O_2} represent the partial pressures of CO and oxygen, a and b are the reaction orders. The experimental date of reaction rate is best fitted with Eq. S5. When b=0, the O_{latt} directly participate in the reaction instead of gas phase oxygen, and the reaction mainly follows the MvK mechanism; the bigger b value indicating that more gaseous oxygen directly

participates in CO oxidation, and the L-H mechanism plays a more important role in reaction.[5, 6]

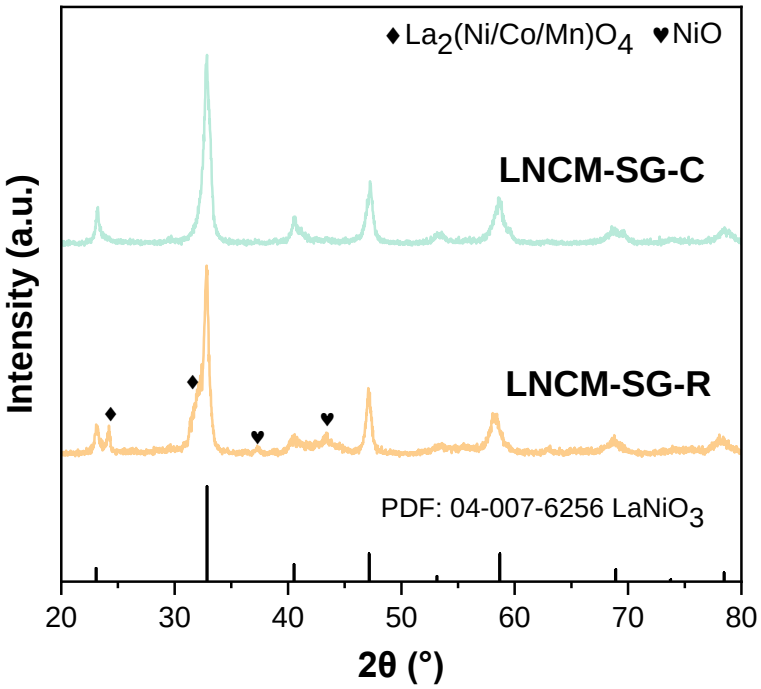

Fig.S16 XRD pattern of LNCM-SG-C and LNCM-SG-R.

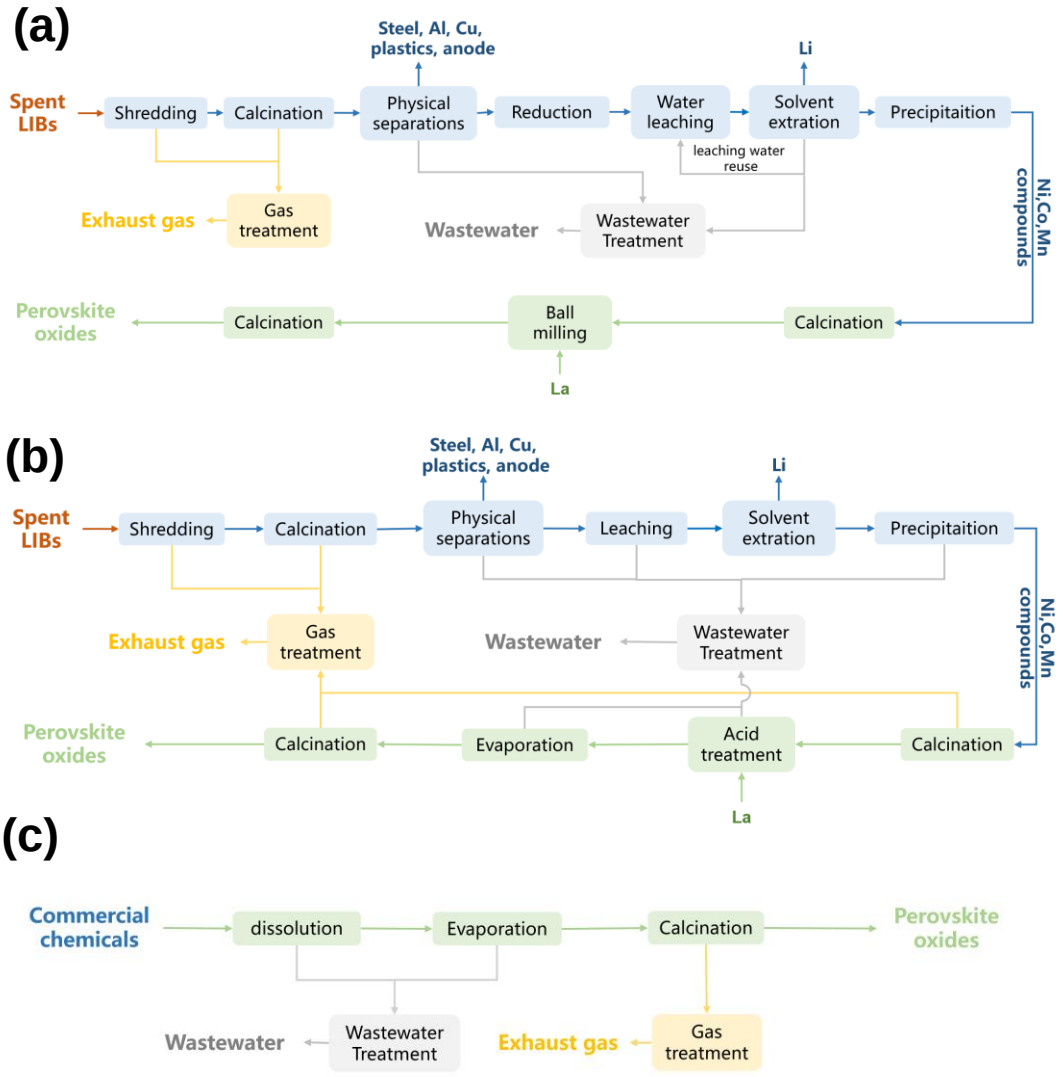

Fig.S17 Process diagram of synthesizing (a) LNCMO-16-600 (b) LNCM-SG-R and (c) LNCM-SG-C

Table S1 Main Composition of NCM

Elements	Ni	Co	Mn	Li	Al
Content (wt.%)	57.70	19.53	18.04	0.7763	0.1073

Table S2 Texture properties of the investigated catalysts

Catalysts	Crystal size (nm) [a]		Avarage particle size (nm) [b]	S_{BET} ($m^2 \cdot g^{-1}$) [c]
	Perovskite	NiO		
LNCM-16-600	9.8	-	29.5	4.28
LNCM-16-800	37.6	-	54.5	1.35
LNCM-16-1000	64.1	-	550	0.64
LNCMO-16-600	8.4	19.6	27	3.29
LNCMO-32-600	10.7	-	35	2.67

[a] The crystal size was calculated by Scherrer equation (Eq. S1).
[b] The average particle size was measured by SEM images.
[c] Specific surface area (S_{BET}) was obtained by BET method.

Table S3 Surface composition of oxygen species derived from XPS analysis.

Catalysts	O species (%)			
	O_{latt}	O_{surf}	O_c	O_{ads}/O_{latt}
LNCM-16-600	24.9	68.2	6.9	2.74
LNCM-16-800	31.9	61.6	6.5	1.93
LNCM-16-1000	36.0	60.4	3.6	1.68
LNCMO-16-600	38.2	55.2	6.6	1.45
LNCMO-32-600	27.4	68.0	4.6	2.48

Table S4 Catalytic CO oxidation performance over different catalysts.

Catalysts	Catalytic CO oxidation performance	
	T_{50} (°C)	T_{90} (°C)
LNCM-16-600	223	309
LNCM-16-800	446	568
LNCM-16-1000	604	747
LNCMO-16-600	192	230
LNCMO-32-600	262	294
LNCM-SG-R	211	234
LNCM-SG-C	237	266

Table S5 The amount of O_2 released (μmol g^{-1}) from each oxygen species and the total O_2 released for catalysts LNCMO-16-600, LNCM-16-600 and LNCMO-32-600 measured through O_2-TPD.

Catalysts	Physiosorbed O_2	O_{ads}	Surface O_{latt}	Bulk O_{latt}	Total O_2 Released
LNCMO-16-600	6.1	81.1	97.2	94.5	278.9
LNCM-16-600	8.3	83.0	56.1	55.6	203.0
LNCMO-32-600	5.4	58.8	53.6	57.3	175.1

Table S6 The amount of H_2 consumption for each peak (mmol g^{-1}) on LNCMO-16-600, LNCM-16-600 and LNCMO-32-600 catalysts.

Catalysts	Peak A	Peak B	Peak C
LNCMO-16-600	0.84	3.57	3.05
LNCM-16-600	0.42	2.57	2.45
LNCMO-32-600	0.30	3.57	2.03

The H_2 consumption peaks < 400 °C, 400-500 °C and > 500 °C is assigned to Peak A, Peak B and Peak C, respectively.

Table S7 Catalytic CO oxidation performance of the perovskite catalysts used in this study and reported in the literature

Catalysts	Preparation method	Reaction condition	T_{50} °C	T_{90} °C	E_a kJ/mol	Ref.
$LaNi_{0.6}Co_{0.2}Mn_{0.2}O_3$	Solid-state	1% CO + 15% O_2 + N_2 balance; GHSV = 30,000 mL $g^{-1}h^{-1}$	192	230	51.2	This work
$LaNi_{0.6}Co_{0.2}Mn_{0.2}O_3$	Solid-state	1% CO + 15% O_2 + N_2 balance; GHSV = 15,000 mL $g^{-1}h^{-1}$	162	197	67.5	This work
$La_{0.9}Ce_{0.05}CoO_3$	Electrospinning	1% CO + 20% O_2 + Ar balance; GHSV = 60,000 mL $g^{-1}h^{-1}$	-	202	92.9	7
$La_{0.3}Sr_{0.7}CoO_{3-\delta}$	Sol-gel	1% CO + 20% O2 + Ar balance; GHSV = 30,000 mL $g^{-1}h^{-1}$	120	-	59.4	8
$Pr_{0.9775}Ag_{0.0225}MnO_{3+\delta}$	Citrate-method	0.5% CO + 5% O_2+ He balance; WHSV=60,000 mL $g^{-1}h^{-1}$	146	225	64.3	9
$La_{0.9}Sr_{0.1}CoO_3$	Templating method	0.4% CO + 10% O_2+ N_2 balance; WHSV=240,000 mL $g^{-1}h^{-1}$	146	186	63.6	10
$SrTi_{0.9}Co_{0.1}O_{3-\delta}$	Solid-state	2% CO+10% O_2+ N_2 balance; WHSV=96,000 mL $g^{-1}h^{-1}$	278	294	70.9	11
$La_{0.4}Sr_{0.6}CoO_{3-\delta}$	Sol-gel	1% CO+20% O_2 + Ar balance; WHSV=60,000 mL $g^{-1}h^{-1}$	-	81	46.6	12
$CuO/SrTiO_3$	Flame spray pyrolysis	2% CO+5% O_2 + N_2 balance; WHSV=60,000 mL $g^{-1}h^{-1}$	127	144	159.33	13
$LaMnO_3$	Templating method	0.2% CO+10% O_2 + N_2 balance; WHSV=60,000 mL $g^{-1}h^{-1}$	-	237	50.5	14

Table S8 Materials requirements (kg) to preparation 1 kg of perovskite oxides through different preparation technologies.

Chemical	Unit Cost ($/kg)	Materials requirements (kg/kg$_{cat}$)		
		LNCMO-16-600	LNCM-SG-C	LNCM-SG-R
Spent Battery (NCM 622)	0	1.157	-	1.102
Ammonium Hydroxide	0.46	-	-	0.039
Hydrochloric Acid	0.15	-	-	0.015
Hydrogen Peroxide	0.74	-	-	0.046
Hydrogen	4.25	0.044	-	-
Sodium Hydroxide	0.4	-	-	0.699
Sulfuric Acid	0.06	-	-	1.350
Soda Ash	0.15	-	-	0.025
Citric Acid	0.69	-	0.782	0.782
Nitric Acid	0.24	-	1.432	1.470
Water	0.00038	1.155	6.030	8.010
Lanthanum Oxide	0.55	0.708	0.699	0.070
Cobalt Oxide	37.66	-	0.060	-
Magnesium Oxide	2.22	-	0.058	-
Nickel sulfate	3.85	-	0.381	-

Table S9 Energy requirements (MJ) to preparation1 kg of perovskite oxides through different preparation technologies.

	Unit Cost ($/MJ)	Energy requirements (MJ/kg_{cat})		
		LNCMO-16-600	LNCM-SG-C	LNCM-SG-R
Diesel	0.0208	0.7	-	0.7
Natural gas	0.0102	2.9	-	2.9
Electricity	0.0191	138.8	59.4	79.5

Table S10 Manufacturing cost details for different production processes of perovskite oxides per year (1,000 tons of perovskite oxides)

	LNCMO-16-600	LNCM-SG-C	LNCM-SG-R
I. Manufacturing Cost, $/year	$15,405,127	$21,528,365	$22,218,618
A. Direct product costs	$6,367,523	$10,215,994	$8,931,276
Raw materials	$629,270	$5,261,185	$2,843,633
Operating labor	$1,065,768	$1,319,365	$1,612,914
Direct supervisory and clerical labor	$159,865	$197,905	$241,937
Utilities	$2,635,422	$1,122,587	$1,561,378
Maintenance and repairs	$1,384,453	$1,682,191	$1,958,539
Operating supplies	$207,668	$252,329	$293,781
Laboratory charges	$106,577	$131,937	$161,291
Patents and royalties	$178,500	$248,496	$257,803
B. Fixed charges	$7,438,953	$9,333,323	$10,867,970
Depreciation	$2,612,175	$3,298,414	$3,840,272
Local taxes	$1,107,562	$1,345,753	$1,566,831
Insurance	$166,134	$201,863	$235,025
Rent	$15,673	$20,582	$25,346
Financing (interest)	$3,537,408	$4,466,712	$5,200,497
C. Plant overhead costs	$1,598,651	$1,979,048	$2,419,371
II. General Expenses, $/year	$2,443,095	$3,327,169	$3,561,640
A. Administrative costs	$479,595	$593,714	$725,811
B. Distribution and selling costs	$1,071,000	$1,490,975	$1,546,816
C. R&D costs	$892,500	$1,242,479	$1,289,013
Total Product Cost, $/year	$17,848,223	$24,849,583	$25,780,262

Table S11 Unit price and amount of co-products

Chemical	Unit Price ($/kg)	Amount of co-product (kg/kg_{cat})		
		LNCMO-16-600	LNCM-SG-C	LNCM-SG-R
Graphite	0.28	0.208	-	0.208
Aluminum	1.3	0.833	-	0.833
Copper	6.6	0.159	-	0.159
Lithium Hydroxide	15.8	0.102	-	-
Lithium Carbonate	12.3	-	-	0.132

REFERENCES

1.J. S. Qiang Dai, Shabbir Ahmed, Linda Gaines, Jarod C. Kelly, Michael Wang *EverBatt: A Closed-loop Battery Recycling Cost and Environmental Impacts Model*, Argonne National Laboratory 2019.

2.P. Xu, Q. Dai, H. Gao, H. Liu, M. Zhang, M. Li, Y. Chen, K. An, Y. S. Meng, P. Liu, Y. Li, J. S. Spangenberger, L. Gaines, J. Lu and Z. Chen, *Joule*, 2020, **4**, 2609-2626.

3.A. Liu, X. Liu, L. Liu, Y. Pu, K. Guo, W. Tan, S. Gao, Y. Luo, S. Yu, R. Si, B. Shan, F. Gao and L. Dong, *ACS Catal.*, 2019, **9**, 7759-7768.

4.Y. Dai, M. Xu, Q. Wang, R. Huang, Y. Jin, B. Bian, C. Tumurbaatar, B. Ishtsog, T. Bold and Y. Yang, *Appl. Catal., B*, 2020, **277**, 119271.

5.R. Kang, X. Wei, F. Bin, Z. Wang, Q. Hao and B. Dou, *Appl. Catal., A*, 2018, **565**, 46-58.

6.A.-P. Jia, G.-S. Hu, L. Meng, Y.-L. Xie, J.-Q. Lu and M.-F. Luo, *J. Catal.*, 2012, **289**, 199-209.

7.S. Liu, W. Zhang, T. Deng, D. Wang, X. Wang, X. Zhang, C. Zhang and W. Zheng, *ChemCatChem*, 2017, **9**, 3102-3106.

8.X. Wang, K. Huang, J. Qian, Y. Cong, C. Ge and S. Feng, *Science Bulletin*, 2017, **62**, 658-664.

9.S. K. Megarajan, S. Rayalu, M. Nishibori, Y. Teraoka and N. Labhsetwar, *ACS Catal.*, 2015, **5**, 301-309.

10.P. Li, X. Chen, Y. Li and J. W. Schwank, *Catal. Today*, 2021, **364**, 7-15.

11.J. Cho, M. Kim, K. T. Park, C. H. Rhee, H. W. Park, B. Koo and J. C. Jung, *Mol. Catal.*, 2023, **550**, 113536.

12.J. Yang, S. Hu, Y. Fang, S. Hoang, L. Li, W. Yang, Z. Liang, J. Wu, J. Hu, W. Xiao, C. Pan, Z. Luo, J. Ding, L. Zhang and Y. Guo, *ACS Catal.*, 2019, **9**, 9751-9763.

13.X. Yuan, L. Meng, Z. Xu, C. Zheng and H. Zhao, *Environ. Sci. Technol.*, 2021, **55**, 14080-14086.

14.W. Si, Y. Wang, Y. Peng and J. Li, *Angew. Chem. Int. Edit.*, 2015, **54**, 7954-7957.